Journal of Zhejiang University-SCIENCE B (Biomedicine & Biotechnology)
ISSN 1673-1581 (Print); ISSN 1862-1783 (Online)
www.jzus.zju.edu.cn; www.springerlink.com
E-mail: jzus@zju.edu.cn

Inhibition of chemotherapy-related breast tumor EMT by application of redox-sensitive siRNA delivery system CSO-ss-SA/siRNA along with doxorubicin treatment*

Xuan LIU, Xue-qing ZHOU, Xu-wei SHANG, Li WANG, Yi LI, Hong YUAN, Fu-qiang HU†‡

College of Pharmaceutical Science, Zhejiang University, Hangzhou 310058, China

†E-mail: hufq@zju.edu.cn

Received Aug. 2, 2019; Revision accepted Oct. 24, 2019; Crosschecked Feb. 22, 2020

Abstract: Metastasis is one of the main reasons causing death in cancer patients. It was reported that chemotherapy might induce metastasis. In order to uncover the mechanism of chemotherapy-induced metastasis and find solutions to inhibit treatment-induced metastasis, the relationship between epithelial-mesenchymal transition (EMT) and doxorubicin (DOX) treatment was investigated and a redox-sensitive small interfering RNA (siRNA) delivery system was designed. DOX-related reactive oxygen species (ROS) were found to be responsible for the invasiveness of tumor cells in vitro, causing enhanced EMT and cytoskeleton reconstruction regulated by Ras-related C3 botulinum toxin substrate 1 (RAC1). In order to decrease RAC1, a redox-sensitive glycolipid drug delivery system (chitosan-ss-stearylamine conjugate (CSO-ss-SA)) was designed to carry siRNA, forming a gene delivery system (CSO-ss-SA/siRNA) down-regulating RAC1. CSO-ss-SA/siRNA exhibited an enhanced redox sensitivity compared to nonresponsive complexes in 10 mmol/L glutathione (GSH) and showed a significant safety. CSO-ss-SA/siRNA could effectively transmit siRNA into tumor cells, reducing the expression of RAC1 protein by 38.2% and decreasing the number of tumor-induced invasion cells by 42.5%. When combined with DOX, CSO-ss-SA/siRNA remarkably inhibited the chemotherapy-induced EMT in vivo and enhanced therapeutic efficiency. The present study indicates that RAC1 protein is a key regulator of chemotherapy-induced EMT and CSO-ss-SA/siRNA silencing RAC1 could efficiently decrease the tumor metastasis risk after chemotherapy.

Key words: Doxorubicin; Tumor metastasis; Ras-related C3 botulinum toxin substrate 1 (RAC1); Epithelial-mesenchymal transition (EMT); Chitosan micelles; Small interfering RNA (siRNA)
https://doi.org/10.1631/jzus.B1900468 **CLC number:** R945

1 Introduction

Tumor metastasis is one of the main reasons causing death in cancer patients (Sun et al., 2017). In recent years, it has been reported that chemotherapeutic drugs may induce metastasis (Ebos, 2015). Cyclophosphamide (CTX) promotes metastases of breast cancer and prostate cancer (Chan et al., 2016; Hung et al., 2017). Paclitaxel (PTX) promotes lung and lymph node metastases of $TLR4^+$ breast cancer (Keklikoglou et al., 2019). Cisplatin or vincristine could enhance liver metastasis of mouse melanoma cells (Karagiannis et al., 2018). The trigger of the metastasis process of chemotherapeutic drugs during treatment may be one of the main causes of tumor metastasis.

‡ Corresponding author
* Project supported by the National Natural Science Foundation of China (No. 81773648), the Zhejiang Provincial Natural Science Foundation of China (No. D19H30001), and the Chinese Postdoc Funding (No. 2018M630686)
ORCID: Xuan LIU, https://orcid.org/0000-0001-6344-8345; Fu-qiang HU, https://orcid.org/0000-0002-9847-134X

The mechanism underlying chemotherapeutic drugs and treatment-induced metastasis is still unclear (Zhao et al., 2017). Some claimed that chemotherapeutic drugs can increase tumor metastasis by stimulating tumor-induced epithelial-mesenchymal transition (EMT) under certain conditions (Quail and Joyce, 2013; Ebos, 2015; Huang et al., 2019). EMT refers to the process by which polar epithelial cells switch to active stromal cells acquiring invasion and migration capabilities. EMT is regarded as an essential step in the tumor metastasis process (Weidenfeld and Barkan, 2018) and could be activated by biological environmental change or chemical stimulation (Liu et al., 2018; Huang et al., 2019). Therefore, it is possible that a chemotherapeutic drug triggers the metastasis process by activating the EMT process of tumor cells. The key protein regulating EMT would be the target for inhibiting chemotherapy-induced metastasis.

Among all the proteins involved in EMT, Ras-related C3 botulinum toxin substrate 1 (RAC1) is a key regulator for cell migration and invasion (Korol et al., 2016; Fu, 2017). RAC1 is an important member of the small G protein Rho (Ras homologue) family. RAC1 binds to nicotinamide adenine dinucleotide phosphate (NADPH) oxidase (NOX) enzymes and is involved in the production of intracellular reactive oxygen species (ROS) (Cadenas, 2018), regulating matrix metalloproteinase-3 (MMP-3) (Zhu et al., 2019). Activated RAC1 protein participates in the formation of actin stress fibers and adhesion plaques, promoting cytoskeleton reorganization (Grobe et al., 2018). Inhibiting the biological function of RAC1 may interrupt the EMT process of tumor cells and decrease metastasis after chemotherapy.

Small interfering RNA (siRNA) can be used to knock down certain proteins such as RAC1. However, siRNA is not stable in vivo, implying that an efficient siRNA delivery vector is needed. Previous studies have found that chitosan stearic grafts, which are biologically safe and degradable, could be utilized as drug carriers (Liu X et al., 2016; Tan et al., 2018). Chitosan stearic grafts have good biocompatibility, strong drug-loading capacity, and high cell uptake rate. The amino groups on chitosan are protonated in aqueous solution, leaving a positive charge on the surface of the glycolipid graft carrier. That makes chitosan stearic grafts able to combine with negatively charged gene drugs such as plasmid DNA (Yan et al., 2013; Wen et al., 2017) and microRNA (miRNA) (Liu J et al., 2016) to construct gene delivery systems. The glycolipid graft carrier can protect the gene drug from ribozyme degradation and improve the efficiency of gene drug transfection by endo-lysosomal escape (Meng et al., 2016; Wen et al., 2017). However, poor intracellular drug release efficiency limited the application of gene delivery systems. It is reported that tumor plasma has a 2–10 times higher level of glutathione (GSH) compared to normal cells (5–10 mmol/L compared to 1–2 mmol/L) (Hu et al., 2015). Therefore, a GSH-responsive drug carrier may improve the drug release efficiency and enhance the therapeutic effect.

In this study, in order to uncover the mechanism of chemotherapy-induced metastasis, the relationship between EMT and doxorubicin (DOX) treatment was investigated. DOX-related ROS and its stimulation of cytoskeleton reconstruction regulated by increased expression of RAC1 were the focus. Chitosan-ss-stearylamine conjugate (CSO-ss-SA), a GSH-sensitive chitosan stearic graft, was designed for siRNA delivery. Physicochemical characterization of CSO-ss-SA/siRNA complexes was studied, including siRNA binding, in vitro GSH-triggered siRNA release, and intracellular gene transport. The efficacy of CSO-ss-SA/siRNA in inhibiting RAC1 protein expression in tumor cells was determined. The effect of CSO-ss-SA/siRNA on the cytoskeletal changes induced by DOX hydrochloride (DOX·HCl) was observed and the inhibition efficacy on chemotherapy-induced tumor cell invasiveness by CSO-ss-SA/siRNA was determined. The animal model of Balb/c nude mice bearing in situ an MCF-7 breast tumor was established to evaluate the efficacy of CSO-ss-SA/siRNA in inhibiting chemotherapy-induced tumor metastasis.

2 Materials and methods

2.1 Materials

DOX·HCl was obtained from Zhejiang Haizheng Pharmaceutical Co., Ltd., China. 2',7'-Dichlorodihydrofluorescein diacetate (DCFH-DA) was purchased from Sigma-Aldrich Co., Ltd. (St. Louis, MO, USA). *N*-acetyl-L-cysteine (NAC) was purchased from Aladdin Industrial Co., Ltd. (Shanghai, China). RAC1/Cdc42 antibody (#4651) was purchased from Cell Signaling Technology Co., Ltd. (Danvers, MA, USA). Fluorescently labeled secondary antibody (Dylight 649-conjugated goat anti-rabbit IgG, GAR6492) was purchased from

Multisciences Co., Ltd. (Hangzhou, China). Rhodamine-B-isothiocyanate (RITC)-labeled phalloidin was obtained from Molecular Probes®, Life Technology (Shanghai, China).

Chitosan oligosaccharide (CSO) with average molecular weight (MW) of 18.0 kDa was prepared by enzymatic degradation of chitosan (CS; 95% acetylate, MW=450.0 kDa; Yuhuan Marine Biochemistry Co., Ltd., Zhejiang, China) as described in previous work (Tan et al., 2018). Stearylamine (SA) was provided by Fluka (Milwaukee, WI, USA). 3,3'-Dithiodipropionic acid (DTPA) was supplied by Tokyo Chemical Industry Co., Ltd. (Tokyo, Japan). *N*-hydroxy succinimide (NHS) and 1-ethyl-3-(3-dimethyl-aminopropyl) carbodiimide hydrochloride (EDC·HCl) were purchased from Shanghai Medpep Co., Ltd. (Shanghai, China). *N*,*N*'-dicyclohexylcarbodiimide (DCC) and 4-dimethylaminepyridine (DMAP) were provided by Shanghai Medped, China. 5-Carboxyfluorescein (FAM)-siRNA and siRNA silencing RAC1 (5'-UGGAGAC ACAUGUGGUAAAGAUAGA-3') were purchased from GenePharma Co., Ltd. (Shanghai, China). Lipofectamine™ 2000 was obtained from Thermo Fisher Scientific (Waltham, MA, USA). All other chemicals were of analytical or chromatographic grade.

2.2 Cell culture

Human breast cancer MCF-7 cells were used as model cells and were cultured in Dulbecco's modified Eagle medium (DMEM) containing 10% (v/v) fetal bovine serum (FBS) with 100 U/mL penicillin and streptomycin at 37 °C under 5% CO_2.

2.3 Cell invasion assay

Transwell assay was used to investigate the effect of chemotherapeutic drug DOX on tumor cell invasiveness. MCF-7 cells were starved in serum-free DMEM culture medium for 24 h. A cell suspension contained 1×10^6 cells/mL in serum-free DMEM containing 0.1% (1 g/L) bovine serum albumin (BSA). The cell suspension (200 μL) was added to the upper chamber of a Transwell plate with pre-packaged Matrigel (filter pore size 8 μm, Corning, Massachusetts, USA). DMEM medium (800 μL) containing 10% (v/v) FBS was added to the lower chamber. After 2 h, DOX·HCl was added. The final concentration of DOX in the upper chamber was 0.20 μg/mL. Twenty-four hours later, crystal purple-stained invasive tumor cells were observed by microscope. ImageJ (National Institutes of Health, Bethesda, MD, USA) was used to count the number of invading cells.

2.4 ROS determination

ROS were determined by using DCFH-DA as a fluorescent probe. After MCF-7 cells were adhered to cell culture plates, DOX·HCl with a final DOX concentration of 0.50 μg/mL was added. Twenty-four hours later, cells were incubated with DCFH-DA. The ROS levels in the cells were then observed by a laser confocal microscopy (Ix81-FV1000, Olympus, Co., Ltd., Japan). In addition, the ROS in tumor cells exposed to DOX (0.10, 0.25, and 0.50 μg/mL) were measured by flow cytometry (FACSCalibur Flow Cytometry, BD Co., Ltd., USA).

2.5 Immunofluorescence staining of RAC1 and cytoskeleton

Immunofluorescence staining was used to determine the expression level of RAC1 protein. MCF-7 cells were seeded into a 24-well cell culture plate at 2×10^4 cells/well. After the cells were attached, DOX·HCl, NAC, and hydrogen peroxide (H_2O_2) were added. Twenty-four hours later, anti-RAC1/Cdc42 antibody and fluorescently labeled secondary antibody were used for staining RAC1, while RITC-labeled phalloidin was used for the cytoskeleton. Hochest 33342 dilution was added to stain the nucleus. The RAC1 protein expression and cytoskeleton of each experimental group were observed under a laser confocal microscope (Ix81-FV1000, Olympus, Co., Japan) and the images were collected.

2.6 Western blot assay for RAC1 expression

MCF-7 cells were cultured in a six-well cell culture plate at 2.5×10^5 cells/well. Different concentrations of DOX·HCl were added. After 24 h, cells were collected and lysated by radio immunoprecipitation assay (RIPA) solution. The solutions were centrifuged at 8000 r/min for 4 min at 4 °C to extract total protein. The expression levels of RAC1 were determined by western blot.

2.7 Synthesis and characterization of CSO-ss-SA

The DTPA method was used to synthesize a disulfide-linked glycoside graft carrier (CSO-ss-SA) (Hu et al., 2015). Octadecylamine (ODA), DTPA, DCC, and DMAP were dissolved in 15 mL anhydrous dimethyl sulfoxide (DMSO), protected with N_2, and

stirred at 150 r/min, 65 °C for 12 h. The mixture was filtered, and EDC and NHS were added to the filtrate and stirred at 65 °C for 0.5 h to obtain a reaction liquid 1. The reaction solution 1 was slowly added to chitosan solution (5.0 mg/mL) with CSO:ODA=5:1 (mol/mol). The mixture was stirred for 8 h to obtain a reaction solution 2. The reaction solution 2 was dialyzed (molecular weight cut off (MWCO) 7 kDa) for 48 h and lyophilized to obtain CSO-ss-SA. The graft was washed with ethanol, redissolved in deionized water, and lyophilized.

The chemical structures of CSO, DTPA, and CSO-ss-SA were confirmed by H^1 nuclear magnetic resonance (NMR) spectroscopy. The amino substitution degree, critical micelle concentration, particle size, and surface potential of CSO-ss-SA were measured.

2.8 Preparation and characterization of CSO-ss-SA/siRNA

siRNA silencing RAC1 protein was selected as the gene drug. The 20 μmol/L siRNA solution was prepared in diethyl pyrocarbonate (DEPC) water, mixed with CSO-ss-SA and siRNA with different ratios of nitrogen to phosphorus (N/P), and vortexed for 30 s. The size distribution and zeta potential of CSO-ss-SA/siRNA complexes were determined by a dynamic light scattering spectrometer (3000HS, Malvern Instruments Ltd., Worcestershire, UK).

2.9 Gel electrophoresis experiments

CSO-ss-SA/siRNA complexes with N/P of 20, 50, 100, 200, 500, and 1000 were prepared. A 1% (w/w) agarose gel containing 0.05% (w/w) ethidium bromide was prepared. CSO-ss-SA/siRNA and loading buffer were mixed and added to sample wells. To evaluate GSH-sensitive gene release capacity, 10 μL of 10 mmol/L GSH Tris-HCl buffer (pH 7.2) was added during preparation of CSO-ss-SA/siRNA. Gel electrophoresis parameters: 100 V, 30 min. Then the gel was observed in an ultraviolet transmission imaging system and images were acquired.

2.10 Cellular uptake

FAM-labeled siRNA was used as a model drug. CSO-ss-SA/FAM-siRNA complexes with N/P ratio of 100 and Lipofectamine™ 2000/FAM-siRNA complexes ("Lipo/FAM-siRNA" for short) were prepared as described before. MCF-7 cells were seeded in 24-well cell culture plates at 5×10^4 cells/well. FAM-siRNA, CSO-ss-SA/FAM-siRNA complexes, and Lipo/FAM-siRNA complexes were added. Twenty-four hours later, the cell nucleus was stained with Hochest 33342 and the images were observed under a laser confocal microscope (Ix81-FV1000, Olympus, Co., Japan).

2.11 Inhibition of RAC1 protein and cytoskeleton by CSO-ss-SA/siRNA

The inhibition efficiency of RAC1 and cytoskeleton by CSO-ss-SA/siRNA was evaluated by immunofluorescence and western blot. DOX·HCl was added to a final concentration of 0.20 μg/mL and incubated for 4 h. CSO-ss-SA/siRNA was added. Lipofectamine™ 2000/siRNA (short as "Lipo/siRNA") was utilized as control. The method is the same as Sections 2.5 and 2.6.

2.12 Cytotoxicity of CSO-ss-SA/siRNA

The cytotoxicity of CSO-ss-SA/siRNA was evaluated by 3-(4,5-dimethylthiazol-2-yl)-2,5 diphenyltetrazolium bromide (MTT) colorimetry. MCF-7 cells were seeded in 96-well plates at 1×10^4 cells/well. Lipo/siRNA was prepared according to the method described before (Meng et al., 2016; Wen et al., 2017). CSO-ss-SA/siRNA and Lipo/siRNA with siRNA content of 100 nmol/L were added. Three sets of parallel experiments were set for each experimental concentration. After 48 h, 15 μL of 5 mg/mL MTT solution was added to each well. The survival rate of tumor cells after Lipo/siRNA and CSO-ss-SA/siRNA treatments was calculated. Cytotoxicities of DOX·HCl and DOX·HCl combined with CSO-ss-SA/siRNA were evaluated by the same method.

2.13 Inhibition of DOX-induced cell invasion by CSO-ss-SA/siRNA in vitro

MCF-7 cells were pre-incubated with CSO-ss-SA/siRNA or Lipo/siRNA containing 100 nmol/L siRNA for 48 h. Transwell experimental model was established according to Section 2.3. After 2 h, DOX·HCl was added to each group with a final concentration of 0.20 μg/mL. Twenty-four hours later the invasive MCF-7 cells in each group were observed. ImageJ was used for quantitative analysis of invasive cells.

2.14 Inhibition of DOX-induced tumor EMT by CSO-ss-SA/siRNA in vivo

All procedures followed were in accordance with the ethical standards of the responsible committee on

animal experimentation of Zhejiang University (Hangzhou, China). An MCF-7 breast cancer in situ tumor-bearing model was constructed with six weeks old female Balb/c nude mice. Estradiol was intramuscularly (i.m.) injected at 0.4 mg/(kg·d) for 3 d. MCF-7 cell suspension was injected into the third pair of nipple fat of Balb/c nude mice at 1×10^7 cells each mouse. Estradiol was added every 5 d after inoculation and supplemented three times. When the tumor volume reached 100 mm^3, mice were injected with DOX·HCl or CSO-ss-SA/siRNA solution. The total amounts of DOX and siRNA injected were 14 mg/kg and 7 mmol/kg, respectively. The date of the first administration was recorded as Day 0. The negative control group was injected with normal saline at 200 μL/d, and the positive control group was injected with DOX·HCl solution at a DOX concentration of 2 mg/(kg·d). The experimental group was injected with DOX·HCl or chitosan oligosaccharide-grafted stearic acid (CSOSA)/DOX at 2 mg/(kg·d) for 7 d. CSO-ss-SA/siRNA was injected at 5 mg/kg siRNA every 3 d from the start of administration.

The tumor growth status was observed. The tumor size and body weight of the mice were monitored. The mice were sacrificed on Day 21. Tumors were dissected and the tumor tissue paraffin-embedded specimens of each experimental group were obtained. Immunohistochemical (IHC) analysis was used to determine EMT transformation markers *E*-cadherin and *N*-cadherin in tumor tissues. Hematoxylin and eosin (H&E) staining was performed. Pictures were observed and collected with an optical microscope. ImageJ was used for image analysis.

2.15 Statistical analysis

All results were repeated in triplicate unless otherwise stated and quantitative data were expressed as mean±standard deviations (SD). Statistical significance was calculated by Student's *t*-test. The statistical significance was defined as a *P*-value less than 0.05.

3 Results

3.1 Chemotherapy-induced tumor cell invasiveness and ROS increase

The effect of a low-concentration chemotherapeutic drug DOX on tumor cell invasiveness was observed by the Transwell chamber method (Hao et al., 2019). As shown in Fig. 1a, DOX promoted the invasion of MCF-7 and A549 cells. The content of ROS in tumor cells was determined by DCFH-DA as a fluorescent probe. Confocal microscopy observation is shown in Fig. 1b. The results of flow cytometry are shown in Fig. 1c. The results showed that DOX significantly enhanced intracellular ROS and the ROS level rose with the increase of drug concentration.

3.2 Chemotherapy-induced RAC1 expression and cytoskeleton reconstruction

The RAC1 protein was labeled by immunofluorescence staining and the expression level of RAC1 in tumor cells was determined after incubation with DOX (Figs. 2a and 2b). When the concentration of DOX was low (0.10–0.20 μg/mL), the expression of RAC1 protein in the cells increased with the concentration of DOX. When the DOX concentration exceeded the half maximal inhibitory concentration (IC_{50}; 0.50 μg/mL), the intracellular RAC1 protein level decreased. The ROS quencher NAC reduced the expression of RAC1 protein, while the ROS promoter H_2O_2 did not significantly increase intracellular RAC1 expression.

The quantitative determination of RAC1 protein by western blot is shown in Fig. 2c. Immuno-fluorescence staining and cytoskeletal staining were performed to observe the regulation of RAC1 induced by a low concentration of DOX on the tumor cytoskeleton (Fig. 3a). The effects of ROS on RAC1 and cytoskeleton were investigated. The results showed that when the concentration of DOX was 0.10 μg/mL, the cytoskeletal strength of MCF-7 increased and the filopodia structure extended. When the concentration of DOX was increased to 0.20 μg/mL, the expression of RAC1 protein was upregulated and the cytoskeleton was enhanced. The expression of DOX-induced RAC1 at a low concentration was shown to be associated with cytoskeletal changes. ROS quencher (10 mmol/L NAC) downregulated RAC1 protein expression (Fig. 3b) and inhibited cytoskeletal reconstruction, while ROS inducer (25 μmol/L H_2O_2) evidently exacerbated cytoskeletal changes and cell deformation.

3.3 Synthesis and structure verification of CSO-ss-SA

In order to form a redox-sensitive siRNA delivery system, a disulfide-linked glycolipid graft carrier (CSO-ss-SA) was designed. CSO-ss-SA was synthesized

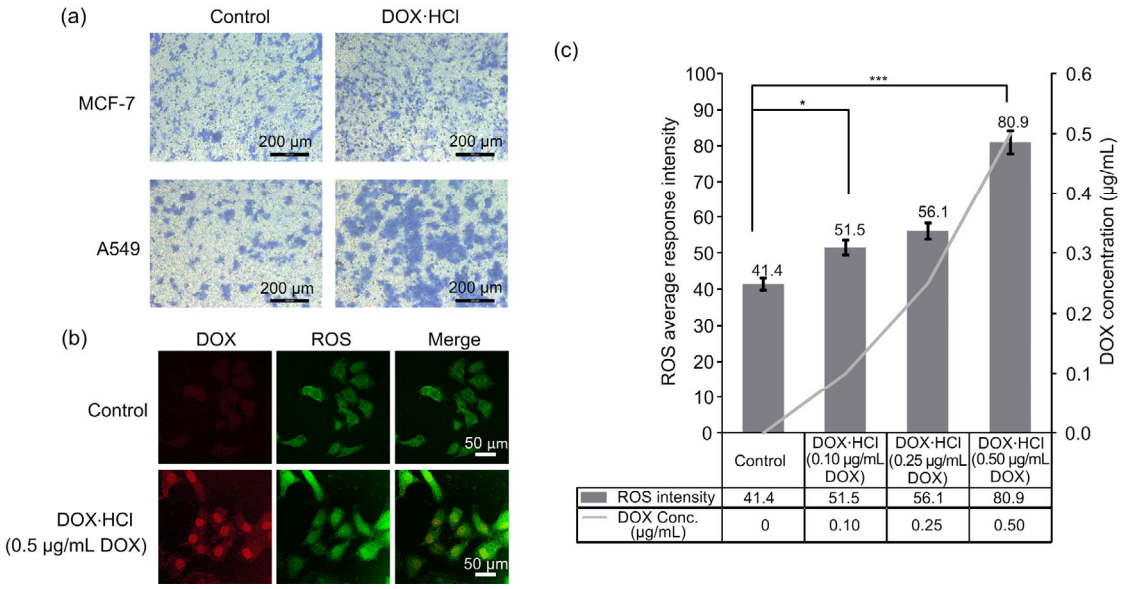

Fig. 1 DOX-induced tumor cell invasion and intracellular ROS production

(a) Transwell assay of tumor cell invasiveness after DOX·HCl treatment. Scale bar: 200 μm. (b) Intracellular ROS observation of MCF-7 cells exposed to DOX·HCL. ROS is represented by green fluorescence. Scale bar: 50 μm. (c) Evaluation of intracellular ROS by flow cytometry. Values are expressed as mean±standard deviation (SD), n=3. Significant difference in respective groups is indicated at $^{*}P<0.05$ and $^{***}P<0.001$. DOX: doxorubicin; HCl: hydrochloride; ROS: reactive oxygen species; Conc.: concentration

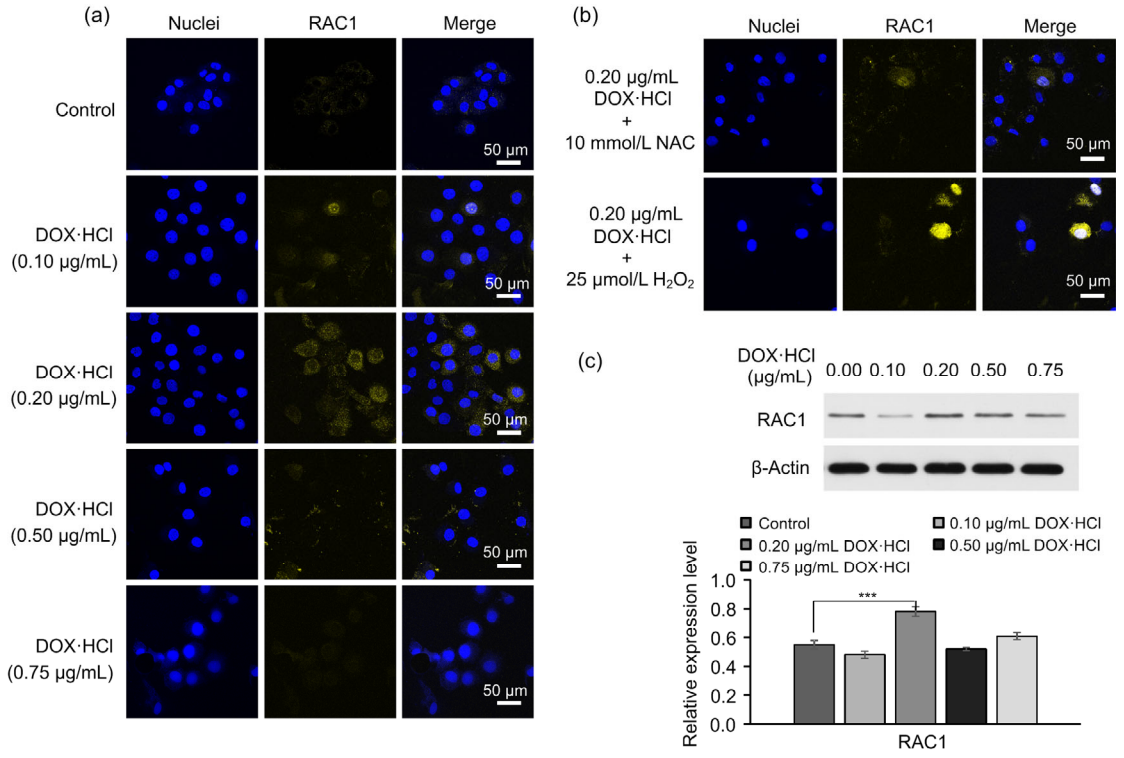

Fig. 2 Influence of DOX and intracellular ROS on RAC1 expression

RAC1 was immunofluorescence stained in MCF-7 cells exposed to DOX·HCl (a) or ROS regulators (b). Cell nucleus is stained blue, and RAC1 is represented in yellow. Scale bar: 50 μm. (c) Quantitative analysis of RAC1 expression level in MCF-7 cells by western blot assay. Values are expressed as mean±standard deviation (SD), n=3. Significant difference in respective groups is indicated at $^{***}P<0.001$. DOX: doxorubicin; HCl: hydrochloride; ROS: reactive oxygen species; NAC: *N*-acetyl-L-cysteine; RAC1: Ras-related C3 botulinum toxin substrate 1

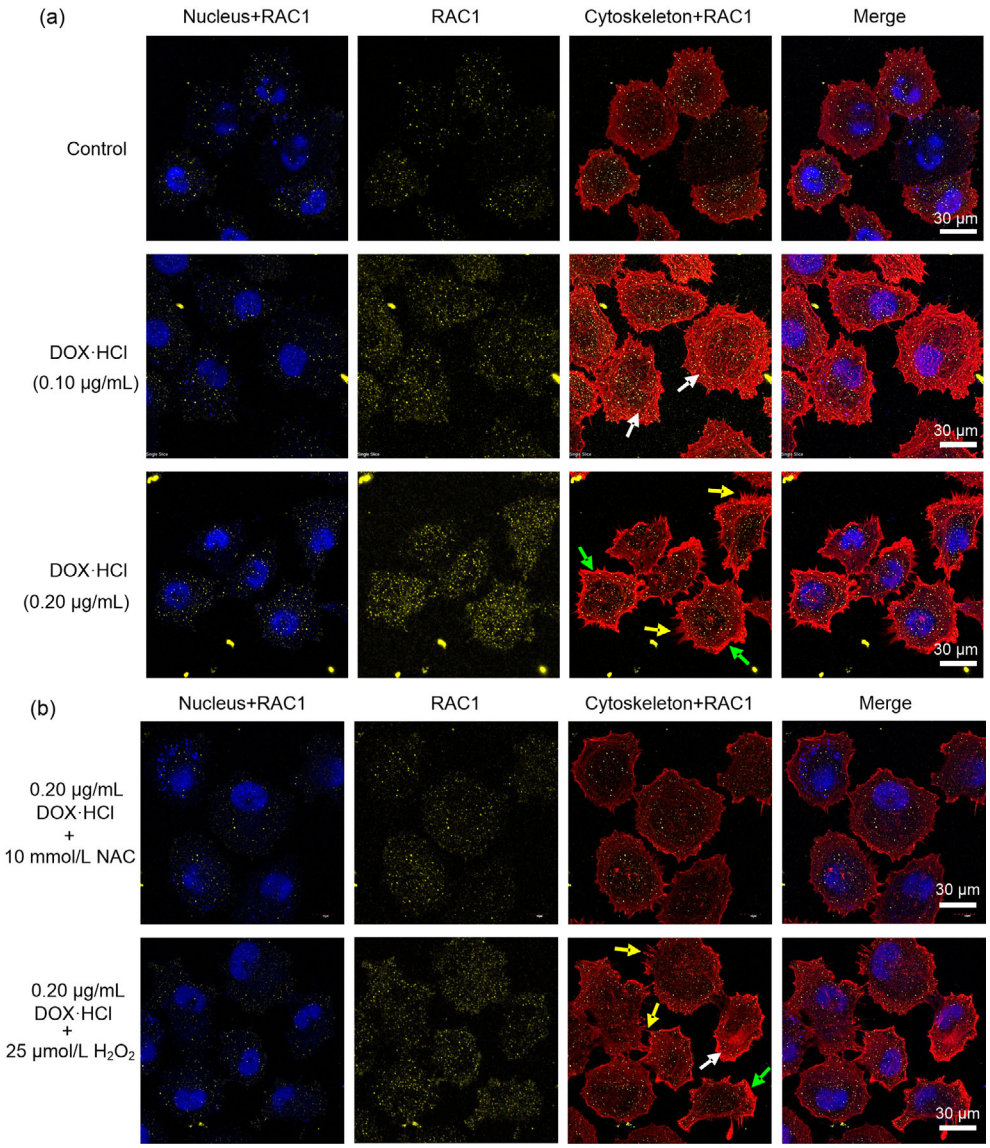

Fig. 3 Influence of DOX on cellular RAC1 expression and cytoskeleton

(a) Regulation of RAC1 induced by a low concentration of DOX on the tumor cytoskeleton. (b) Effects of ROS on RAC1 and cytoskeleton. Cell nucleus is stained blue, RAC1 is represented in yellow, and cytoskeleton is labeled red. Yellow arrow: filopodia; Green arrow: stress fiber; White arrow: pseudopod. Scale bar: 30 μm. DOX: doxorubicin; HCl: hydrochloride; ROS: reactive oxygen species; RAC1: Ras-related C3 botulinum toxin substrate 1; NAC: *N*-acetyl-L-cysteine

by DTPA method. The synthetic route is shown in Fig. 4a. Under the protection of N_2, DTPA was dehydrated with an amino group on stearylamine (ODA) forming an amide bond to obtain an intermediate product.

Then, under the action of EDC and NHS, the intermediate product reacted with the amino group on the chitosan to obtain CSO-ss-SA. The product, a sponge-like water-soluble solid, was purified and obtained by lyophilization.

H^1 NMR was used to confirm the chemical structure of CSO-ss-SA. The H^1 NMR spectrum of CSO-ss-SA (Fig. 4b) showed that the peak with a chemical shift of 0.78 ppm (1 ppm=1×10^{-6}) was assigned to 0.93 ppm of $-CH_3$ on ODA. The peak of 1.20 ppm was attributed to $-CH_2-$ on ODA. The peak between 2.20 ppm and 2.80 ppm was attributed to DTPA. The peaks of 1.93 ppm and 2.21 ppm were attributed to $-CH_3$ and $-NH_2$ of CSO, respectively. The above

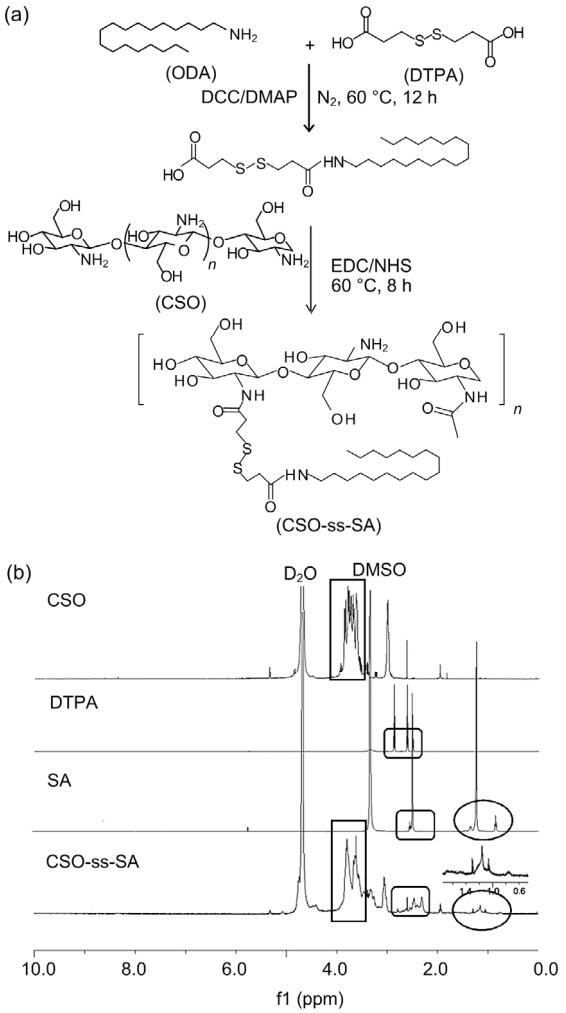

Fig. 4 Synthesis and structure verification of CSO-ss-SA
(a) Synthesis route of CSO-ss-SA. (b) H^1 NMR spectrum of CSO-ss-SA and synthetic materials. The peak with a chemical shift of 0.78 ppm (ellipses) was assigned to 0.93 ppm of $-CH_3$ on ODA. The peak between 2.20 ppm and 2.80 ppm was attributed to DTPA (small rectangles). CSO-ss-SA: chitosan-ss-stearylamine conjugate; ODA: octadecylamine; DTPA: 2-carboxyethyl disulfide; DCC: *N*,*N*′-dicyclohexylcarbodiimide; DMAP: 4-dimethylaminepyridine; EDC: 1-ethyl-3-(3-dimethyl-aminopropyl) carbodiimide hydrochloride; NHS: *N*-hydroxy succinimide; DMSO: dimethyl sulfoxide; H^1 NMR: nuclear magnetic resonance spectroscopy. 1 ppm=1×10^{-6}

results showed that the ODA was linked to DTPA and definitely grafted with CSO.

3.4 Physicochemical characteristics of CSO-ss-SA

The amino substitution degree, critical micelle concentration, particle size, and surface potential meter of CSO-ss-SA were measured. The amino substitution degree of CSO-ss-SA was (8.67±1.12)%. The critical micelle concentration of CSO-ss-SA measured by the pyrene fluorescence probe method was (43.7±4.3) μg/mL. The critical micelle concentration (CMC) of the graft micelles is small, indicating that the graft micelles have high stability in aqueous media. The particle diameter and zeta surface potential of CSO-ss-SA were (142.9±3.2) nm and (8.9±0.7) mV, respectively. The results showed that CSO-ss-SA exhibited high water solubility, strong micelle ability in water, and homogeneous micelle size. The surface of CSO-ss-SA was positively charged, making it a potential carrier for negatively charged siRNA.

3.5 Preparation and characterization of CSO-ss-SA/siRNA complexes

In order to form CSO-ss-SA/siRNA complexes, CSO-ss-SA and siRNA solution were vortexed at room temperature. Particle size and surface potential of CSO-ss-SA/siRNA complexes with N/P of 20, 50, 100, 200, 500, and 1000 were measured. As shown in Table 1, with the increase of N/P ratio, the surface potential of the composite gradually increased while the particle size first rose and then decreased. When N/P<100, the surface potential of the composite was negative and the particle size varied with N/P ratio. When N/P=50, the composite particle size reached a maximum value of (224.9±4.2) nm. When N/P≥100, the surface potential of the composite was positive and the particle size decreased as N/P increased.

CSO-ss-SA/siRNA complexes with N/P of 20, 50, 100, 200, 500, and 1000 were screened. Gel electrophoresis assay was used to determine the binding ability between CSO-ss-SA and siRNA (Fig. 5a). The siRNA is negatively charged under physiological conditions and can form a self-assembled complex by electrostatic adsorption with a positively charged glycolipid graft. In the gel electrophoresis assay, the siRNA released from the CSO-ss-SA/siRNA would move to the anode under the action of the electric field force and the sample band in the gel could be seen under ultraviolet imaging, while the siRNA combined with CSO-ss-SA would stay in the sample well. Fig.5a showed that, when N/P<100, the electrophoresis band of siRNA was still visible in the gel, indicating that the siRNA was not completely combined with CSO-ss-SA. When N/P≥100, there was no siRNA band in the gel, showing the complete contact between siRNA and CSO-ss-SA. Subsequent experiments were performed using CSO-ss-SA/siRNA complexes with N/P=100.

Table 1 Particle size and surface potential of CSO-ss-SA/siRNA complexes

Complexes with different N/P	Average particle size (nm)	PI	Zeta potential (mV)
CSO-ss-SA	142.9±3.2	0.132±0.002	8.9±0.7
CSO-ss-SA/siRNA$_{N/P=20}$	167.3±2.8	0.128±0.011	−7.6±0.3
CSO-ss-SA/siRNA$_{N/P=50}$	224.9±4.2	0.117±0.025	−2.4±0.2
CSO-ss-SA/siRNA$_{N/P=100}$	191.3±1.7	0.092±0.012	0.1±0.8
CSO-ss-SA/siRNA$_{N/P=200}$	153.9±5.3	0.210±0.030	10.8±0.3
CSO-ss-SA/siRNA$_{N/P=500}$	103.3±7.9	0.363±0.037	23.9±0.4
CSO-ss-SA/siRNA$_{N/P=1000}$	98.6±6.3	0.614±0.027	31.7±0.5

Each test was repeated in parallel three times for mean±standard deviation (SD). CSO-ss-SA: chitosan-ss-stearylamine conjugate; N/P: nitrogen to phosphorus; PI: isoelectric point

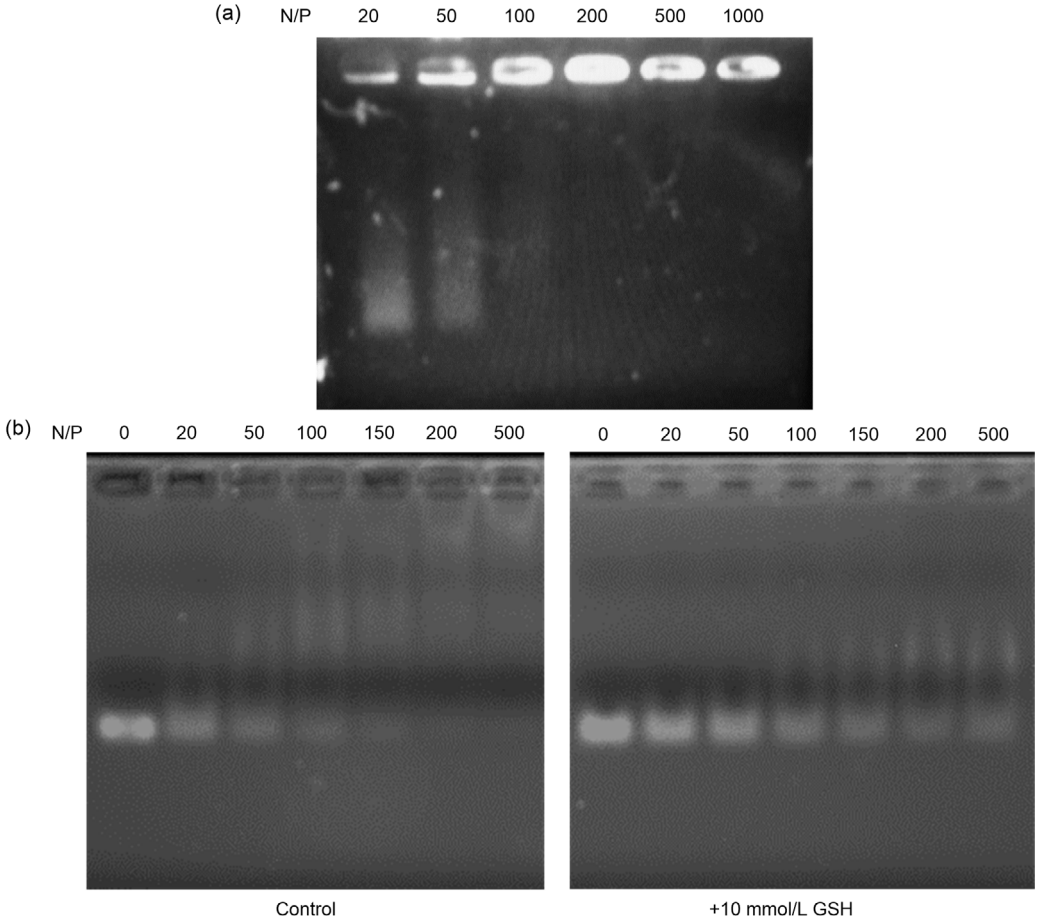

Fig. 5 Gel electrophoresis assay and GSH-triggered siRNA release of CSO-ss-SA/siRNA complexes

(a) Gel electrophoresis assay of CSO-ss-SA/siRNA with a series of N/P ratio. (b) GSH-triggered siRNA release evaluation. The siRNA complexes were pre-incubated with 10 mmol/L GSH for 30 min. CSO-ss-SA/siRNA was unable to retain siRNA in the wells in an environment containing 10 mmol/L GSH. This was significantly different from the control group. CSO-ss-SA/siRNA exhibited redox-sensitive release of siRNA under reducing conditions. N/P: nitrogen to phosphorus; CSO-ss-SA: chitosan-ss-stearylamine conjugate; GSH: glutathione

3.6 GSH-triggered siRNA release

The in vitro reduction-sensitive release of CSO-ss-SA/siRNA complexes was evaluated by gel electrophoresis assay under 10 mmol/L GSH (Fig. 5b).

3.7 Cellular uptake of CSO-ss-SA/siRNA

Human breast cancer MCF-7 cells were used as model cells. CSO-ss-SA/FAM-siRNA complexes with N/P ratio of 100 were selected with Lipo/FAM-siRNA as the positive control and FAM-siRNA as the negative control. The FAM green fluorescence can only be observed when the FAM-siRNA was successfully taken up by the cells. As shown in Fig. 6a, MCF-7 cells incubated with FAM-siRNA showed no green fluorescence, indicating that the siRNA itself could not be directly taken by cells. However, a large amount of green fluorescence was observed in cells incubated with CSO-ss-SA/FAM-siRNA and Lipo/FAM-siRNA, indicating that CSO-ss-SA can effectively deliver siRNA into MCF-7 tumor cells.

3.8 Inhibition of RAC1 by CSO-ss-SA/siRNA in vitro

RAC1 expression inhibition efficiency of CSO-ss-SA/siRNA was evaluated by western blot assay (Figs. 6b and 6c). DOX·HCl (0.20 μg/mL) was added to each group previously to increase the expression of RAC1 protein in MCF-7 cells. It was shown that CSO-ss-SA/siRNA reduced the expression of RAC1 protein by 38.2% after incubation for 48 h. This is similar to the effect of Lipo/siRNA. At the same time, immunofluorescence staining of RAC1 and cytoskeleton staining were performed on MCF-7 cells. The inhibitory effects of CSO-ss-SA/siRNA on DOX-induced RAC1 expression and tumor cytoskeletal reconstruction were observed (Fig. 6d). Pre-incubation of CSO-ss-SA/siRNA or Lipo/siRNA reduced the expression of RAC1 protein and inhibited the upregulation of RAC1 protein by DOX, consistent with the results in western blot assays (Figs. 6b and 6c).

The cytoskeleton staining of each experimental group showed that 0.20 μg/mL DOX·HCl could induce untreated MCF-7 cells to extend filopodia (yellow arrow; Fig. 6d) and thicken pseudopod (white arrow; Fig. 6d). MCF-7 cells incubated with CSO-ss-SA/siRNA or Lipo/siRNA showed little change in DOX-induced cytoskeleton changes and only Lipo/siRNA-treated MCF-7 cells extended short filopodia (yellow arrow; Fig. 6d). Low concentration of DOX could upregulate RAC1 protein, induce cytoskeletal changes, enhance the motility of tumor cells, and promote EMT transformation of tumor cells. It was shown in Fig. 6d that CSO-ss-SA/siRNA downregulated RAC1 and inhibited DOX-induced tumor cytoskeleton reconstruction, suggesting that CSO-ss-SA/siRNA could inhibit tumor cell motility, block the EMT process, and reduce the risk of tumor metastasis after chemotherapy.

3.9 Cytotoxicity of CSO-ss-SA/siRNA complexes combined with DOX in vitro

The cytotoxicity of CSO-ss-SA/siRNA was evaluated by MTT assay. Lipo/siRNA was utilized as control (Fig. 7a). After incubation for 24 h, CSO-ss-SA/siRNA showed no significant cytotoxicity to MCF-7 cells, indicating that CSO-ss-SA/siRNA is a safer drug carrier than Lipo/siRNA. The RAC1 protein is not directly related to the apoptotic pathway of tumor cells or suicide signaling pathways such as autophagy. Therefore, CSO-ss-SA/siRNA does not affect the survival rate of tumor cells directly by regulating RAC1.

The effect of incubation of CSO-ss-SA/siRNA on the cytotoxicity of DOX·HCl was also determined by MTT assay (Fig. 7b). The cells were pre-incubated with CSO-ss-SA/siRNA containing 100 nmol/L siRNA for 24 h and different concentrations of DOX·HCl were added. CSO-ss-SA/siRNA did not have a significant effect on DOX·HCl cytotoxicity. Transwell assay was used to evaluate the influence of CSO-ss-SA/siRNA on chemotherapy-induced tumor metastasis (Figs. 7c and 7d). Untreated MCF-7 cells increased invasiveness with 0.20 μg/mL DOX·HCl, while MCF-7 cells pre-incubated with CSO-ss-SA/siRNA or Lipo/siRNA showed less invasiveness. It was shown that the number of invasive tumor cells induced by DOX was reduced by 42.5% since CSO-ss-SA/siRNA downregulated the expression of RAC1 protein.

3.10 Therapy efficiency of CSO-ss-SA/siRNA complexes combined with DOX in vivo

An animal model of Balb/c nude mice bearing in situ MCF-7 breast tumor was established. The tumor growth inhibition and EMT interrupt effect of CSO-ss-SA/siRNA combined with DOX·HCl were studied. The tumor inhibition rate and tumor growth curves are shown in Figs. 8b and 8d, respectively. The changes in body weight during the experiment are shown in Fig. 8c. The results showed that the tumor inhibition rates of

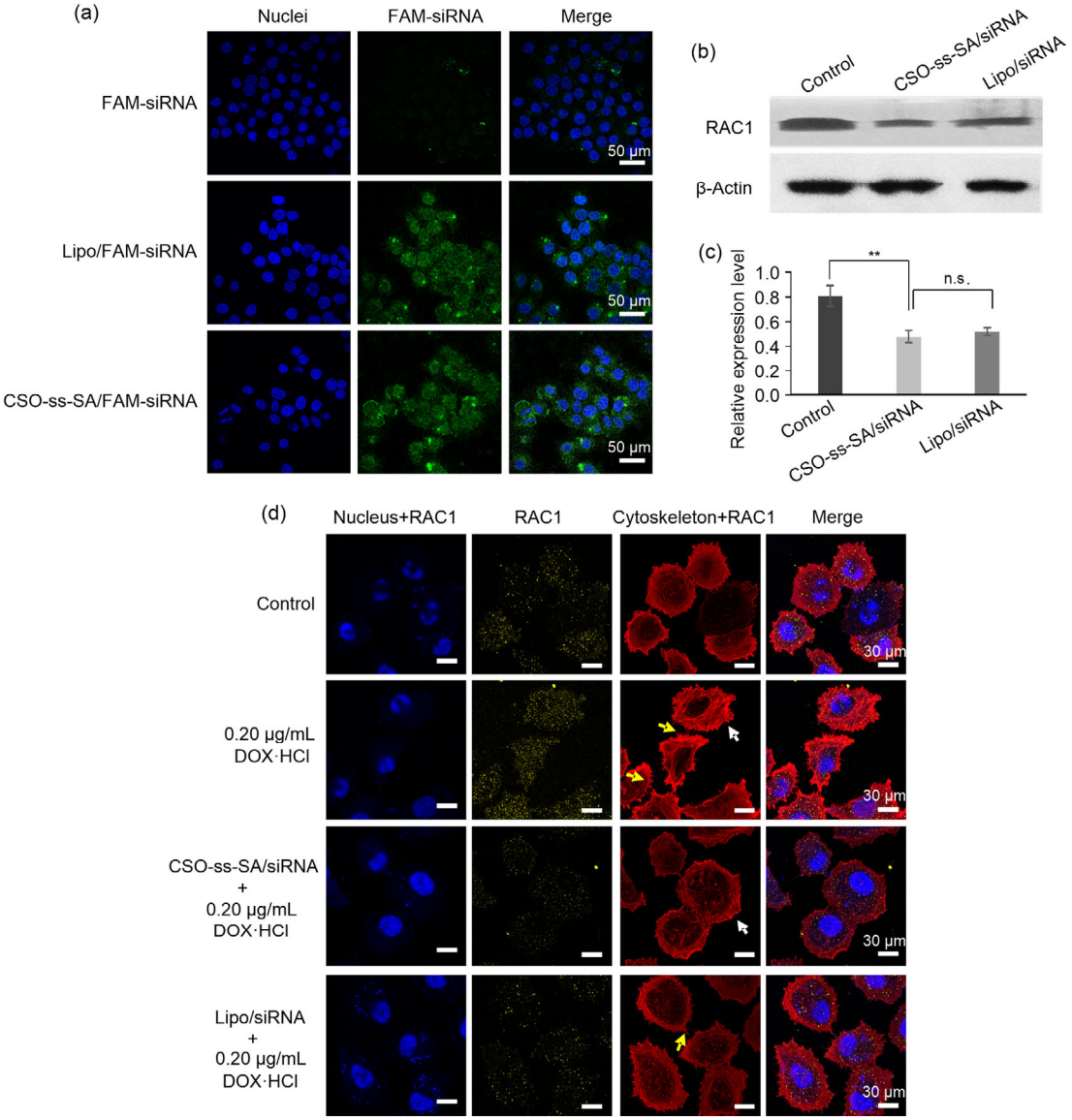

Fig. 6 Cellular uptake of CSO-ss-SA/siRNA and regulation of RAC1 and cytoskeleton by CSO-ss-SA/siRNA

(a) Cellular uptake of the siRNA complexes. siRNA is green fluorescence. Cell nucleus is blue. Scale bar: 50 μm. (b) Western blot assay for cellular RAC1 expression. (c) Quantitative analysis of (b). Values are expressed as mean±standard deviation (SD), n=3. Significant difference between groups is indicated as $^{**}P<0.01$. (d) The regulation of RAC1 and cytoskeleton by siRNA complexes represented by immunofluorescence staining. Cell nucleus is blue, RAC1 is yellow, and cytoskeleton is red. Yellow arrow: filopodia; White arrow: pseudopod. Scale bar: 30 μm. FAM/siRNA: FAM-labeled siRNA complexes; Lipo/FAM-siRNA: Lipofectamine™ 2000/FAM-siRNA complexes; Lipo/siRNA: Lipofectamine™ 2000/siRNA; CSO-ss-SA: chitosan-ss-stearylamine conjugate; RAC1: Ras-related C3 botulinum toxin substrate 1; DOX: doxorubicin; HCl: hydrochloride; n.s.: not significant

DOX·HCl, CSO-ss-SA/siRNA, and CSO-ss-SA/siRNA combined with DOX·HCl were 82.45%, 23.59%, and 84.76%, respectively, exhibiting the enhanced anti-tumor activity by CSO-ss-SA/siRNA combined with DOX·HCl.

Immunohistochemistry experiments were conducted to investigate the efficacy of CSO-ss-SA/siRNA in inhibiting DOX-induced tumor EMT (Fig. 8e). Downregulation of *E*-cadherin and upregulation of *N*-cadherin are hallmarks of tumor EMT transformation.

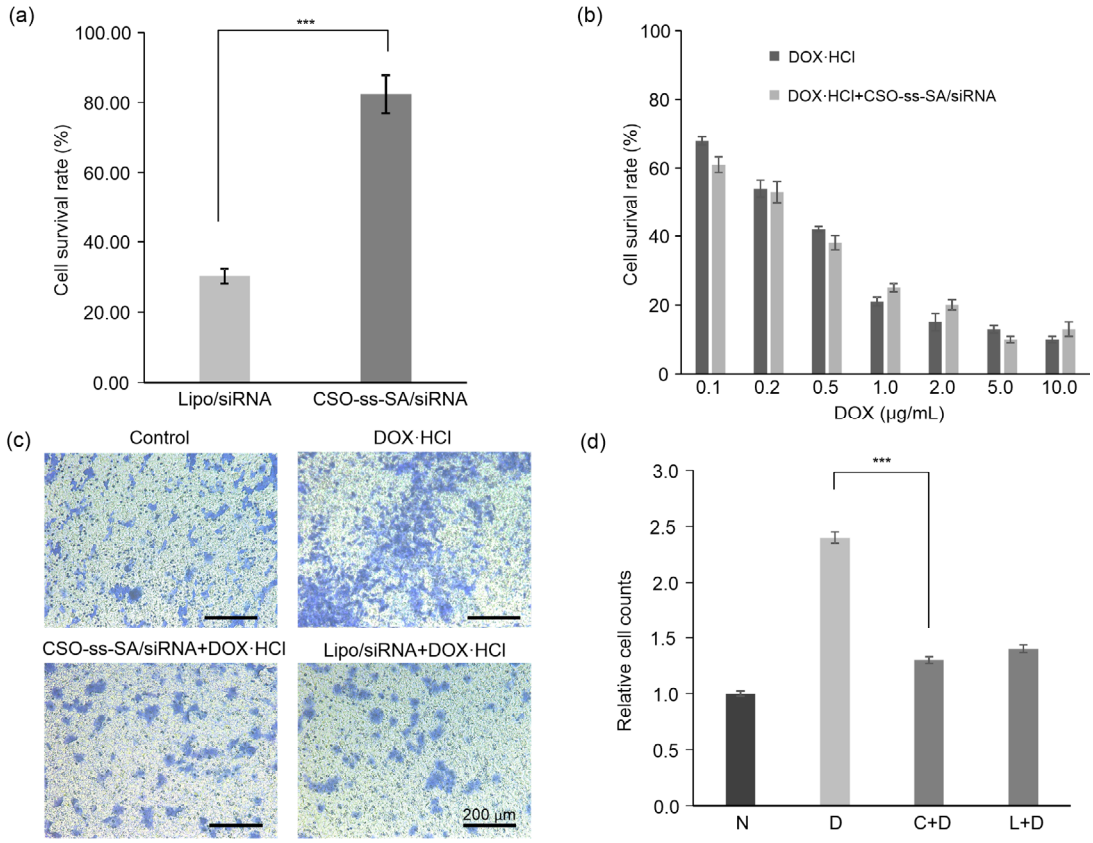

Fig. 7 Cytotoxicity and invasiveness inhibition effect of CSO-ss-SA/siRNA

(a) Cytotoxicity of Lipo/siRNA and CSO-ss-SA/siRNA. (b) Cytotoxicity of DOX·HCl combined with CSO-ss-SA/siRNA. (c) Transwell assay of MCF-7 cells exposed to DOX·HCl or DOX·HCl combined with siRNA complexes. Scale bar: 200 μm. (d) Quantitative analysis of results in (c). N: control group; D: DOX·HCl group; C+D: CSO-ss-SA/siRNA+DOX·HCl group; L+D: Lipo/siRNA+DOX·HCl group. Values are expressed as mean±standard deviation (SD), n=3. Significant difference in respective groups is indicated at $^{***}P<0.001$. CSO-ss-SA: chitosan-ss-stearylamine conjugate; Lipo/siRNA: Lipofectamine™ 2000/siRNA; DOX: doxorubicin; HCl: hydrochloride

The tumor tissue treated by DOX·HCl alone exhibited an obviously EMT feature. After CSO-ss-SA/siRNA treatment, there was no obvious downregulation of *E*-cadherin or upregulation of *N*-cadherin in the tumor tissue after DOX treatment. It is suggested that CSO-ss-SA/siRNA could inhibit the tumor EMT transformation induced by the chemotherapeutic drug DOX.

4 Discussion

Tumor metastasis is one of the main reasons causing death in cancer patients. It has been reported that chemotherapeutic drugs may induce metastasis (Ebos, 2015). The anthracycline chemotherapeutic drug DOX can be inserted into DNA base pairs in the nucleus of tumor cells, inhibiting the synthesis of nucleic acids and leading the cells to death. However, the process of DOX-induced tumor cell metastasis is still not elucidated.

In the cell plasma, DOX will form an unstable DOX-semiquinone structure, releasing ROS under the action of NOX enzyme (NADPH oxidase), triggering lipid peroxidation, damaging the cell membrane or DNA, and leading to cell apoptosis (Polyakov et al., 2018). ROS produced by DOX may bring chemical pressure to cells. This chemical pressure might cause EMT, which is regarded as the beginning of the metastasis process. Therefore, the ROS increase by DOX might be a possible cause of DOX-induced

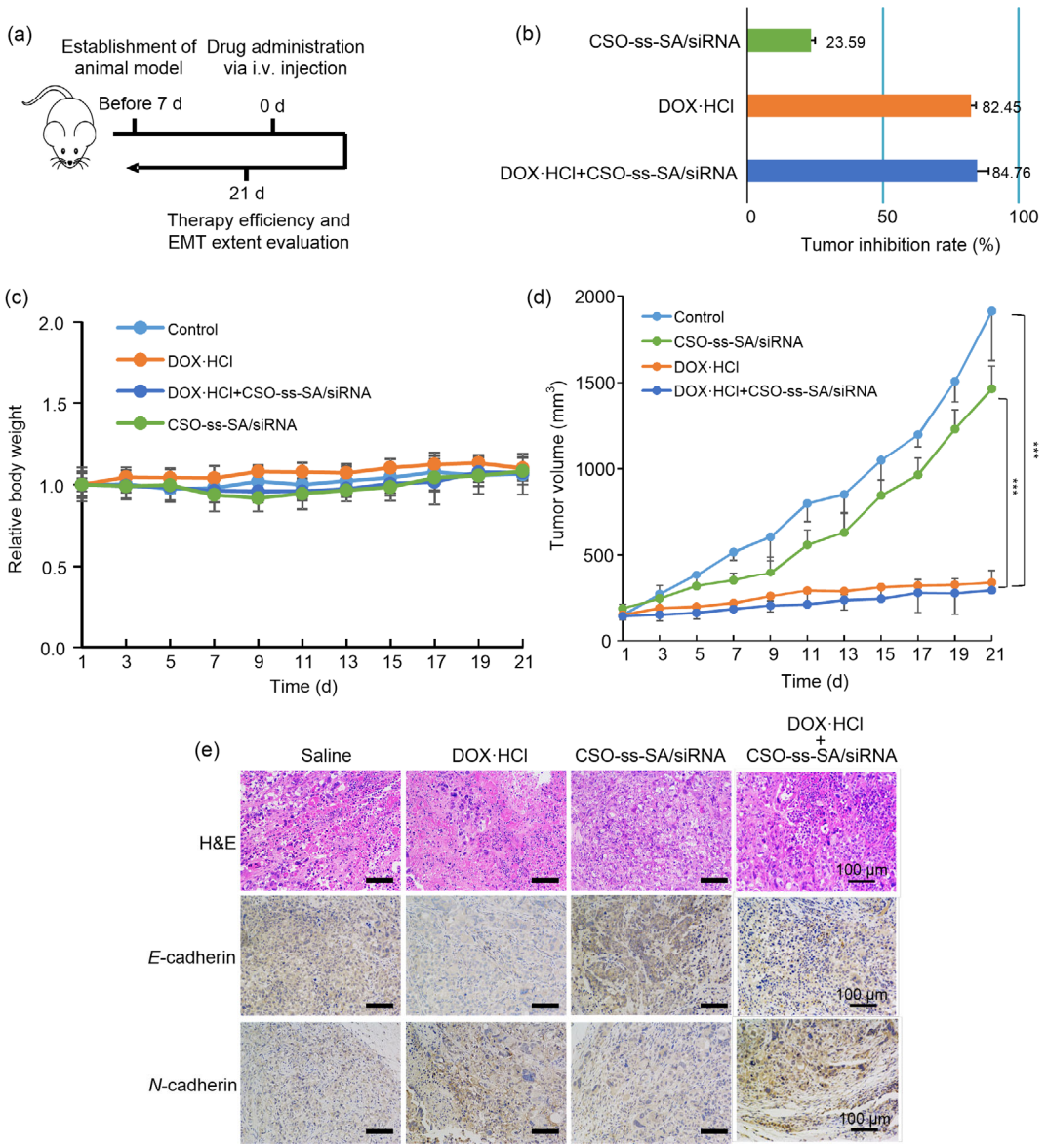

Fig. 8 Therapy efficiency of CSO-ss-SA/siRNA combined with DOX·HCl in vivo

(a) Procedure of animal experiments. An animal model of Balb/c nude mice bearing in situ MCF-7 breast tumor was established (n=5). Drugs were injected via intravenous (i.v.) injection when the tumor volume reached 100 mm^3. (b) Tumor inhibition rate calculated by tumor weight. (c) Body weight changing curve of mice during the experiments. (d) Tumor volume changing curve during the experiments. Values are expressed as mean±standard deviation (SD), n=3. Significant difference in respective groups is indicated at $^{***}P$<0.001. (e) IHC assay for EMT marker and H&E staining in the tumor tissues. Scale bar: 100 μm. EMT: epithelial-mesenchymal transition; CSO-ss-SA: chitosan-ss-stearylamine conjugate; DOX: doxorubicin; HCl: hydrochloride; IHC: immunohistochemical analysis; H&E: hematoxylin-eosin

metastatic growth of tumor cells. The key protein regulating EMT would be the target for inhibiting chemotherapy-induced metastasis.

RAC1 protein is an important member of the small G protein Rho (Ras homologue) family. Activated RAC1 protein could participate in the formation of actin stress fibers and adhesion plaques, promoting cytoskeletal structure reorganization (Grobe et al., 2018). In this study, low concentration of DOX upregulated RAC1 protein expression while NAC, a ROS quencher, inhibited the expression of RAC1 induced by DOX. It indicates that the expression of

RAC1 protein could be regulated by DOX-related ROS. High concentration of DOX did not promote the upregulation of RAC1 protein expression. It may be due to the degradation of protein and DNA in a high ROS concentration condition (Mirzaei et al., 2018). Therefore, RAC1 is an important protein that regulates ROS-induced tumor cell metastasis and cell motility changes. Thus, an efficient drug aiming at regulating RAC1 expression might have a chance to inhibit DOX-induced EMT.

Delivering siRNA into the ROS raised cells is a possible solution for downregulating RAC1. The effective release of gene drugs in tumor cells is a prerequisite for an efficacy of siRNA delivery systems. Previous studies have found that gene drug delivery systems constructed with CSOSA exhibited delayed gene delivery, resulting in lower transfection efficiency (Meng et al., 2016). Therefore, a gene delivery carrier with enhanced drug release efficiency was need. According to previous study, the GSH concentration in tumor cells is 10 mmol/L, which is remarkably higher than that in normal cells (Liu et al., 2019). The GSH-sensitive disulfide bond allowed CSO-ss-SA to become biodegradable in a high GSH level condition. When N/P=100, the potential of complexes was close to 0 mV. The charge attraction between the glycolipid graft carrier and the siRNA was the weakest, making CSO-ss-SA an efficient redox-sensitive siRNA carrier. The physicochemical characteristics of CSO-ss-SA showed that it was a potential siRNA carrier.

RAC1 protein is widely distributed in human cells and encoded by the *RAC1* gene (Vaquero and Fouassier, 2016; De et al., 2019). Once siRNA is delivered into tumor cells, it would form an RNA-induced silencing complex (RISC) with various proteins such as helicase and adenosine triphosphate (ATP). RISC binds to homologous complementary messenger RNA (mRNA) and degrades it, making the gene silenced. At the same time, siRNA can also use mRNA as a template to generate new siRNA under the action of RNA-dependent RNA polymerase (RdRP) and continue to play its role. In this study, after CSO-ss-SA/siRNA delivered siRNA (5'-UGGAGACACAU GUGGUAAAGAUAGA-3') for RAC1 protein into tumor cells, siRNA achieved a silencing effect on the *RAC1* gene and inhibited expression of RAC1 protein.

The cytotoxicity of the redox-sensitive gene delivery system was determined by MTT assay. The results showed that CSO-ss-SA/siRNA was safe to MCF-7 cells when decreasing the expression of RAC1 protein. CSO-ss-SA/siRNA could obviously inhibit the cytoskeleton reconstruction and invasiveness enhancement by decreasing RAC1 expression in MCF-7 cells. Furthermore, in vivo studies showed that CSO-ss-SA/siRNA definitely inhibited tumor EMT induced by DOX.

However, the long-time therapeutic influence of CSO-ss-SA/siRNA combined with DOX or CSOSA/DOX has not been investigated in this research. The influence on protein expression or cell factor secretion after treatment is still unknown. Since EMT is regarded as the beginning of tumor metastasis, it is believed that CSO-ss-SA/siRNA, which could inhibit tumor tissue EMT efficiently, should be a promising therapy method to inhibit breast tumor metastasis and prolong the survival time of breast tumor patients. This will be the focus of our next research.

5 Conclusions

In this study, we found that low concentration of DOX could increase tumor cell invasiveness and promote EMT in tumors. RAC1 protein was related to the DOX-induced EMT. CSO-ss-SA, as an efficient redox-sensitive carrier for delivering siRNA silencing RAC1 into tumor cells, reduced the expression of RAC1 by 38.2% and decreased DOX-induced tumor invasion cells by 42.5% in vitro. Furthermore, CSO-ss-SA/siRNA inhibited DOX-induced tumor EMT in vivo. In conclusion, the RAC1 protein is a key regulator of chemotherapy-induced metastasis and CSO-ss-SA/siRNA silencing RAC1 could effectively decrease the tumor metastasis risk after chemotherapy.

Contributors

Xuan LIU performed the experimental research and data analysis, wrote and edited the manuscript. Xue-qing ZHOU performed the data analysis and participated in the paperwork. Xu-wei SHANG contributed in polymer synthesis. Li WANG contributed in image analysis. Yi LI collected and analyzed the data. Hong YUAN and Fu-qiang HU contributed in the study design. All authors have read and approved the final manuscript, have full access to all the data in the study, and take responsibility for the integrity and security of the data.

Compliance with ethics guidelines

Xuan LIU, Xue-qing ZHOU, Xu-wei SHANG, Li WANG, Yi LI, Hong YUAN, and Fu-qiang HU declare that they have no conflict of interest.

All institutional and national guidelines for the care and use of laboratory animals were followed.

References

Cadenas S, 2018. ROS and redox signaling in myocardial ischemia-reperfusion injury and cardioprotection. *Free Radic Biol Med*, 117:76-89. https://doi.org/10.1016/j.freeradbiomed.2018.01.024

Chan TS, Hsu CC, Pai VC, et al., 2016. Metronomic chemotherapy prevents therapy-induced stromal activation and induction of tumor-initiating cells. *J Exp Med*, 213(13): 2967-2988. https://doi.org/10.1084/jem.20151665

De P, Aske JC, Dey N, 2019. RAC1 takes the lead in solid tumors. *Cells*, 8(5):382. https://doi.org/10.3390/cells8050382

Ebos JML, 2015. Prodding the beast: assessing the impact of treatment-induced metastasis. *Cancer Res*, 75(17):3427-3435. https://doi.org/10.1158/0008-5472.can-15-0308

Fu XD, 2017. Both sides of the same coin: Rac1 splicing regulation by EGF signaling. *Cell Res*, 27(4):455-456. https://doi.org/10.1038/cr.2017.19

Grobe H, Wüstenhagen A, Baarlink C, et al., 2018. A Rac1-FMNL2 signaling module affects cell-cell contact formation independent of Cdc42 and membrane protrusions. *PLoS ONE*, 13(3):e0194716. https://doi.org/10.1371/journal.pone.0194716

Hao LG, Rong W, Bai LJ, et al., 2019. Upregulated circular RNA circ_0007534 indicates an unfavorable prognosis in pancreatic ductal adenocarcinoma and regulates cell proliferation, apoptosis, and invasion by sponging miR-625 and miR-892b. *J Cell Biochem*, 120(3):3780-3789. https://doi.org/10.1002/jcb.27658

Hu YW, Du YZ, Liu N, et al., 2015. Selective redox-responsive drug release in tumor cells mediated by chitosan based glycolipid-like nanocarrier. *J Control Release*, 206:91-100. https://doi.org/10.1016/j.jconrel.2015.03.018

Huang D, Cao L, Xiao L, et al., 2019. Hypoxia induces actin cytoskeleton remodeling by regulating the binding of CAPZA1 to F-actin via PIP2 to drive EMT in hepatocellular carcinoma. *Cancer Lett*, 448:117-127. https://doi.org/10.1016/j.canlet.2019.01.042

Hung CM, Hsu YC, Chen TY, et al., 2017. Cyclophosphamide promotes breast cancer cell migration through CXCR4 and matrix metalloproteinases. *Cell Biol Int*, 41(3):345-352. https://doi.org/10.1002/cbin.10726

Karagiannis GS, Condeelis JS, Oktay MH, 2018. Chemotherapy-induced metastasis: mechanisms and translational opportunities. *Clin Exp Metastasis*, 35(4):269-284. https://doi.org/10.1007/s10585-017-9870-x

Keklikoglou I, Cianciaruso C, Güç E, et al., 2019. Chemotherapy elicits pro-metastatic extracellular vesicles in breast cancer models. *Nat Cell Biol*, 21(2):190-202. https://doi.org/10.1038/s41556-018-0256-3

Korol A, Taiyab A, West-Mays JA, 2016. RhoA/ROCK signaling regulates TGFβ-induced epithelial-mesenchymal transition of lens epithelial cells through MRTF-A. *Mol Med*, 22(1):713-723. https://doi.org/10.2119/molmed.2016.00041

Liu J, Meng T, Yuan M, et al., 2016. MicroRNA-200c delivered by solid lipid nanoparticles enhances the effect of paclitaxel on breast cancer stem cell. *Int J Nanomed*, 11:6713-6725. https://doi.org/10.2147/ijn.s111647

Liu X, Cheng BL, Meng TT, et al., 2016. Synthesis and biological application of BKT-140 peptide modified polymer micelles for treating tumor metastasis with an enhanced cell internalization. *Polym Chem*, 7(7):1375-1386. https://doi.org/10.1039/C5PY01807B

Liu XX, Liu WD, Wang L, et al., 2018. Roles of flotillins in tumors. *J Zhejiang Univ-Sci B (Biomed & Biotechnol)*, 19(3):171-182. https://doi.org/10.1631/jzus.B1700102

Liu ZL, Shen N, Tang ZH, et al., 2019. An eximious and affordable GSH stimulus-responsive poly(α-lipoic acid) nanocarrier bonding combretastatin A4 for tumor therapy. *Biomater Sci*, 7(7):2803-2811. https://doi.org/10.1039/C9BM00002J

Meng TT, Wu J, Yi HX, et al., 2016. A spermine conjugated stearic acid-g-chitosan oligosaccharide polymer with different types of amino groups for efficient p53 gene therapy. *Coll Surf B-Biointerf*, 145:695-705. https://doi.org/10.1016/j.colsurfb.2016.05.071

Mirzaei S, Hadadi Z, Attar F, et al., 2018. ROS-mediated heme degradation and cytotoxicity induced by iron nanoparticles: hemoglobin and lymphocyte cells as targets. *J Biomol Struct Dyn*, 36(16):4235-4245. https://doi.org/10.1080/07391102.2017.1411832

Polyakov N, Leshina T, Fedenok L, et al., 2018. Redox-active quinone chelators: properties, mechanisms of action, cell delivery, and cell toxicity. *Antiox Redox Signal*, 28(15): 1394-1403. https://doi.org/10.1089/ars.2017.7406

Quail DF, Joyce JA, 2013. Microenvironmental regulation of tumor progression and metastasis. *Nat Med*, 19(11):1423-1437. https://doi.org/10.1038/nm.3394

Sun T, Wang GF, Zhang Y, 2017. Primary splenic carcinosarcoma with local invasion of chest wall: a rare case. *J*

Zhejiang Univ-Sci B (Biomed & Biotechnol), 18(8):717-722. https://doi.org/10.1631/jzus.B1700262

Tan YN, Zhu Y, Zhao Y, et al., 2018. Mitochondrial alkaline pH-responsive drug release mediated by celastrol loaded glycolipid-like micelles for cancer therapy. *Biomaterials*, 154:169-181. https://doi.org/10.1016/j.biomaterials.2017.07.036

Vaquero J, Fouassier L, 2016. Rac1 and EMT: a dangerous liaison? *Transl Cancer Res*, 5(Suppl 7):S1483-S1485. https://doi.org/10.21037/tcr.2016.12.42

Weidenfeld K, Barkan D, 2018. EMT and stemness in tumor dormancy and outgrowth: are they intertwined processes? *Front Oncol*, 8:381. https://doi.org/10.3389/fonc.2018.00381

Wen LJ, Tan YN, Dai SH, et al., 2017. VEGF-mediated tight junctions pathological fenestration enhances doxorubicin-loaded glycolipid-like nanoparticles traversing BBB for glioblastoma-targeting therapy. *Drug Deliv*, 24(1):1843-1855. https://doi.org/10.1080/10717544.2017.1386731

Yan JJ, Du YZ, Chen FY, et al., 2013. Effect of proteins with different isoelectric points on the gene transfection efficiency mediated by stearic acid grafted chitosan oligosaccharide micelles. *Mol Pharm*, 10(7):2568-2577. https://doi.org/10.1021/mp300732d

Zhao M, Ding XF, Shen JY, et al., 2017. Use of liposomal doxorubicin for adjuvant chemotherapy of breast cancer in clinical practice. *J Zhejiang Univ-Sci B (Biomed & Biotechnol)*, 18(1):15-26. https://doi.org/10.1631/jzus.B1600303

Zhu Y, Yan L, Zhu WJ, et al., 2019. MMP2/3 promote the growth and migration of laryngeal squamous cell carcinoma via PI3K/AKT-NF-κB-mediated epithelial-mesenchymal transformation. *J Cell Physiol*, 234(9):15847-15855. https://doi.org/10.1002/jcp.28242

中文概要

题　目：RAC1 蛋白靶向氧化还原敏感型 siRNA 递释系统抑制化疗诱导乳腺肿瘤转移的研究

目　的：探明 RAC1 蛋白调控阿霉素（DOX）诱导肿瘤转移机制，设计靶向 RAC1 的小干扰 RNA（siRNA）递释系统，抑制 DOX 治疗诱导的肿瘤皮质间质样（EMT）转化。

创新点：探明了 DOX 通过 RAC1 蛋白诱导肿瘤细胞发生转移性变化的机制，构建了靶向沉默 RAC1 蛋白的 siRNA 递释系统，有效降低了 DOX 化疗后肿瘤组织转移的风险。

方　法：选用 MCF-7 细胞为模型细胞，体外考察 DOX 相关活性氧（ROS）对 RAC1 蛋白的调控作用。针对肿瘤细胞内高谷胱甘肽（GSH）浓度的氧化还原条件，选用二硫键为敏感桥链，壳聚糖为亲水性骨架，硬脂胺为疏水基团，构建氧化还原敏感型基因药物载体 CSO-ss-SA。选择靶向沉默 RAC1 的 siRNA 为模型药物，构建基因药物递释系统 CSO-ss-SA/siRNA。考察 CSO-ss-SA/siRNA 的理化性质、体外敏感释放及细胞摄取。通过免疫荧光染色法、蛋白免疫印迹法和细胞侵袭性实验考察基因药物递释系统的细胞药效。选用 Balb/c 裸鼠构建 MCF-7 乳腺肿瘤原位荷瘤动物模型，考察 CSO-ss-SA/siRNA 对 DOX 治疗诱导肿瘤组织 EMT 转化的抑制作用。

结　论：RAC1 是 DOX 诱导细胞侵袭性的关键蛋白。靶向沉默 RAC1 的 siRNA 基因递释系统可在体内外有效抑制 DOX 治疗诱导的肿瘤组织 EMT 转化，降低化疗诱导转移的风险。

关键词：阿霉素（DOX）；肿瘤转移；RAC1；皮质间质样转化（EMT）；壳聚糖胶束；小干扰 RNA（siRNA）